Available online at www.sciencedirect.com
ScienceDirect
Catalysis Today 130 (2008) 292–301
CATALYSIS TODAY
www.elsevier.com/locate/cattod

Deep HDS over NiMo/Zr-SBA-15 catalysts with varying MoO_3 loading

Oliver Y. Gutiérrez [a], Fernando Pérez [a], Gustavo A. Fuentes [b], Xim Bokhimi [c], Tatiana Klimova [a,*]

[a] *Facultad de Química, Universidad Nacional Autónoma de México (UNAM), Cd. Universitaria, Coyoacán, México D.F. 04510, Mexico*
[b] *Área de Ingeniería Química, Universidad Autónoma Metropolitana-Iztapalapa (UAM-I), Av. Michoacán y Purísima, Iztapalapa, México D.F. 09340, Mexico*
[c] *Instituto de Física, Universidad Nacional Autónoma de México (UNAM), Apartado Postal 20364, México D.F. 01000, Mexico*

Available online 3 December 2007

Abstract

In the present work, with the aim of searching for new, highly effective catalysts for deep HDS, a series of NiMo catalysts with different MoO_3 loadings (6–30 wt.%) was prepared using SBA-15 material covered with ZrO_2-monolayer as a support. Prepared catalysts were characterized by N_2 physisorption, small- and wide-angle XRD, UV–vis diffuse reflectance spectroscopy, temperature-programmed reduction, SEM-EDX and HRTEM, and their catalytic activity was evaluated in the 4,6-dimethyldibenzothiophene hydrodesulfurization (HDS). It was observed that ZrO_2 incorporation on the SBA-15 surface improves the dispersion of the Ni-promoted oxidic and sulfided Mo species, which were found to be highly dispersed, up to 18 wt.% of MoO_3 loading. Further increase in metal charge resulted in the formation of MoO_3 crystalline phase and an increase in the stacking degree of the MoS_2 particles. All NiMo catalysts supported on ZrO_2-modified SBA-15 material showed high activity in HDS of 4,6-DMDBT. The best catalyst having 18 wt.% MoO_3 and 4.5 wt.% NiO was almost twice more active than the reference NiMo/γ-Al_2O_3 catalyst. High activity of NiMo/Zr-SBA-15 catalysts and its evolution with metal loading was related to the morphological characteristics of the MoS_2 active phase determined by HRTEM.

Keywords: SBA-15; Mesoporous molecular sieves; Zirconia; NiMo catalysts; Deep hydrodesulfurization; 4,6-Dimethyldibenzothiophene

1. Introduction

A growing interest in the removal of sulfur from gasoline and diesel oil by means of deep hydrodesulfurization (HDS) is due to the implementation of more stringent fuel specifications in order to reduce exhaust emissions. The requirement of production of ultra-clean diesel fuel with low sulfur content (less than 50 ppm) makes imperative the development of new hydrotreating catalysts, highly active and selective for hydrodesulfurization (HDS) of the refractory polyaromatic sulfur compounds [1–3]. In order to achieve this goal, different approaches have been tried, for example, the use of novel supports (carbon, TiO_2, TiO_2–Al_2O_3, MCM-14, etc.) and of novel active phases (noble metals, transition metal phosphides, etc.) or the search for new promoters and additives for the conventional HDS catalysts [4–7]. Development of novel supports seems to be an interesting and practical option because the support nature and characteristics play an important role in the catalytic activity. So far, different materials have been tried as supports for Mo (or W) active phases promoted by Ni (or Co). It was found that the support can influence catalyst reducibility or sulfidability, structure and dispersion of the deposited metal oxides, as well as the morphology of the sulfided active phases [8].

Among different materials evaluated recently as supports for HDS catalysts, mesoporous molecular sieves of SBA-type [9,10], have attracted attention. These materials have high hydrothermal stability, and their textural properties are better than those of the traditional γ-alumina support. Purely siliceous SBA-15 materials have already been tested as supports for unpromoted Mo(W) catalysts or Co(Ni) promoted ones. Thus, Sampieri et al. [11] reported on the preparation of Mo/SBA-15 catalysts with various Mo loadings (9, 14 and 20 wt.%) by thermal spreading of MoO_3. These catalysts showed higher catalytic activity in dibenzothiophene HDS than the reference Mo/Al_2O_3 catalyst, and the activity was found to increase with the Mo loading up to 14 wt.% Mo. Murali Dhar et al. [12] evaluated the catalytic activity of Mo/SBA-15 catalysts with 2–12 wt.% Mo loadings, prepared by a standard incipient

* Corresponding author. Tel.: +52 55 56225371; fax: +52 55 56225371.
E-mail address: klimova@servidor.unam.mx (T. Klimova).

0920-5861/$ – see front matter © 2007 Elsevier B.V. All rights reserved.
doi:10.1016/j.cattod.2007.10.110

wetness impregnation method, in HDS of thiophene and hydrogenation (HYD) of cyclohexene. It was also observed that SBA-15-supported catalysts were 2–2.5 times more active compared to γ-Al_2O_3-supported formulations. In addition, the catalytic activities for both HYD and HDS increased up to 8 wt.% Mo and decreased at higher loadings. Vradman et al. [13] used purely siliceous SBA-15 as a support for preparing high loading NiW catalysts by sonication. In this case, the best catalyst was 1.4 times more active in dibenzothiophene HDS and 7.3 times more active in toluene HYD than a sulfided commercial Co–Mo/Al_2O_3. All above results clearly show the advantages of the SBA-15 materials in comparison with the conventionally used alumina supports. It should be mentioned that these promising results were obtained with purely siliceous SBA-15, even though it is well-known that the interactions between silica and Mo (or W) species are very weak and lead to a low and inhomogeneous dispersion of the sulfided active phases [14].

In order to overwhelm the drawbacks of purely siliceous SBA-15 support and improve its interaction with HDS active species, it was proposed to modify SBA-15 with different heteroatoms (Al, Ti, Zr). Muthu Kumaran et al. [15] synthesized Mo, CoMo and NiMo catalysts supported on Al-containing SBA-15 materials with different Si/Al ratios (10–40). Aluminum (III) incorporation in the support increased Mo dispersion and catalytic activities in thiophene HDS and cyclohexene HYD. In our group, NiMo catalysts were prepared using as supports SBA-15 materials modified with titanium (IV) or zirconium (IV) oxides [16,17]. These catalysts showed high performance in HDS of 4,6-dimethyldibenzothiophene (4,6-DMDBT), one of the most refractory sulfur compounds. TiO_2 and ZrO_2 loading in the support produced an increase in the activity, being ZrO_2-containing NiMo/SBA-15 catalysts more active than those containing TiO_2. Improvement of the catalytic activity was attributed to an increase in the dispersion of Ni and Mo species due to their stronger interaction with titania and, especially, zirconia-containing supports [16]. Titania or zirconia incorporation in the SBA-15 resulted also in the promotion of the hydrogenation pathway of 4,6-DMDBT hydrodesulfurization, which was related with the morphology of MoS_2 crystallites on TiO_2 or ZrO_2-covered supports. Murali Dhar et al. [18] prepared SBA-15 materials modified with various amounts (10–50 wt.%) of ZrO_2 nanoparticles by urea hydrolysis method and tested them as supports for Mo, CoMo and NiMo catalysts. Catalytic activities of these catalysts for thiophene HDS and cyclohexene HYD were evaluated as a function of ZrO_2 content in SBA-15. It was noted that both HDS and HYD activities increase up to 25 wt.% of zirconia and decrease with further increase in ZrO_2 loading.

Resuming above results, it can be concluded that the modification of the SBA-15 material by the incorporation of heteroatoms (Al, Ti, Zr) improves the interaction of the support with the deposited metal species (Ni, Mo), increasing by this means support ability to disperse HDS active phases and, consequently, catalytic activities for HDS and HYD. In above cited works [15–18], catalysts with relatively low metal loadings (∼12 wt.% MoO_3 and ∼3 wt.% CoO (or NiO)) were prepared. To our knowledge, up to now there are no reports about the use of heteroatom-modified SBA-15 materials in the preparation of high metal loading HDS catalysts.

In the present work, with the aim of searching for new, highly effective catalysts for deep HDS, a series of NiMo/Zr-SBA-15 catalysts with different MoO_3 loadings (6–30 wt.%) was prepared. Zr-SBA-15 material, used as a support, was synthesized by chemical grafting at room temperature and contained 23 wt.% of highly dispersed ZrO_2 species. Supports and catalysts were characterized and tested in 4,6-dimethyldibenzothiophene HDS reaction.

2. Experimental

2.1. Support and catalyst preparation

The purely siliceous SBA-15 material used in this paper has been synthesized according to the procedure described elsewhere [9,10]. The triblock copolymer Pluronic P123 (M_{av} = 5800, $EO_{20}PO_{70}EO_{20}$, Aldrich) was used as the structure-directing agent and tetraethyl orthosilicate (TEOS) as the silica source. The nominal molar ratio of the chemicals used in the synthesis was 1TEOS:0.017P123:5.95HCl:171H_2O. Zirconia-modified SBA-15 support (Zr-SBA-15) was prepared by chemical grafting [16] using zirconium (IV) propoxide (Zr(*n*-PrO)$_4$, 70 wt.% solution in 1-propanol, Aldrich) as the zirconia source, and dry ethanol as the solvent (EtOH, Aldrich, 99,999%). In the grafting procedure, calcined SBA-15 was slurried in dry EtOH containing Zr(*n*-PrO)$_4$ (2.5 g per 1.0 g of SBA-15) for 8 h at room temperature. To eliminate excess of Zr(*n*-PrO)$_4$, the filtered material was washed three times with dry EtOH. The solid was then dried in air at room temperature and calcined in static air at 550 °C for 5 h.

NiMo catalysts supported on Zr-SBA-15 were prepared by a standard incipient wetness technique. The calcined Zr-SBA-15 support was impregnated successively using aqueous solutions of ammonium heptamolybdate, $(NH_4)_6Mo_7O_{24}{\cdot}4H_2O$ (Aldrich), and nickel nitrate, $Ni(NO_3)_2{\cdot}6H_2O$ (Aldrich). Mo was impregnated first. After each impregnation, the catalysts were dried (100 °C, 24 h) and calcined (500 °C, 4 h). NiMo(*X*)/Zr-SBA-15 catalysts with different MoO_3 loadings (*X* = 6–30 wt.% of MoO_3) and constant MoO_3/NiO weight ratio equal to 4 were prepared. In addition NiMo catalysts with 12 wt.% MoO_3 and 3 wt.% NiO supported on purely siliceous SBA-15 and γ-Al_2O_3 were prepared for comparison purposes. These reference catalysts will be denoted as NiMo/SBA-15 and NiMo/γ-Al_2O_3, respectively.

2.2. Support and catalyst characterization

The supports and catalysts were characterized by N_2 physisorption, small-angle and wide-angle X-ray diffraction (XRD), isoelectric point (IEP), SEM-EDX, UV–vis diffuse reflectance spectroscopy (DRS), temperature-programmed reduction (TPR) and HRTEM. N_2 adsorption/desorption isotherms were measured with a Micromeritics ASAP 2000 automatic analyzer at liquid N_2 temperature. Prior to the

experiments, the samples were degassed ($p < 10^{-1}$ Pa) at 270 °C for 6 h. Specific surface areas were calculated by the BET method (S_{BET}), the total pore volume (V_p) was determined by nitrogen adsorption at a relative pressure of 0.98 and pore size distributions from both the adsorption and the desorption isotherms by the BJH method. The mesopore diameters (D_{ads} and D_{des}) correspond to the maxima of the pore size distributions obtained from adsorption and desorption isotherms, respectively. The micropore area (S_μ) was estimated using the correlation of t-Harkins & Jura (t-plot method). Wide-angle XRD patterns were recorded in the $3^\circ \leq 2\theta \leq 90^\circ$ range on a Siemens D5000 diffractometer, using Cu Kα radiation (λ = 1.5406 Å) and a goniometer speed of $1^\circ(2\theta)$ min^{-1}. Small-angle XRD ($2\theta = 1$–10°) was performed on a Bruker D8 Advance diffractometer using small divergence and scattering slits of 0.05°. The measurements of zeta potential of SBA-15-type supports were carried out at different pH values in a Zeta Meter 3.0+ instrument. Isoelectric point (IEP) was determined as the pH value at which zeta potential of the support particles was found to be equal to 0. Chemical composition of supports and catalysts was determined by SEM-EDX using JEOL 5900 LV microscope with OXFORD ISIS equipment. UV–vis–NIR electronic spectra of the samples were recorded in the wavelength range 200–2500 nm using a Cary |5E| spectrophotometer equipped with a diffuse reflectance attachment. $BaSO_4$ was used as reference. TPR experiments were carried out in an automated ISRI-RIG-100 characterization system equipped with a TC detector. In the TPR experiments, the samples were pretreated *in situ* at 500 °C for 2 h under air flow and cooled in an Ar stream. The reduction step was performed with an Ar/H_2 mixture, with a heating rate of 10 °C/min, up to 1000 °C. High resolution transmission electron microscopy (HRTEM) studies were performed using a Jeol 2010 microscope (resolving power 1.9 Å). The solids were ultrasonically dispersed in heptane and the suspension was collected on carbon coated grids. HRTEM pictures were taken from different parts of the same sample dispersed on the microscope grid.

2.3. Catalytic activity

The 4,6-DMDBT HDS activity tests were performed in a batch reactor at 300 °C and 7.3 MPa total pressure for 8 h. Prior to the catalytic activity evaluation, the catalysts were sulfided *ex situ* in a tubular reactor at 400 °C for 4 h in a stream of 15 vol.% of H_2S in H_2 under atmospheric pressure. The course of the reaction was followed by withdrawing aliquots each hour and analyzing them on an HP-6890 chromatograph. To corroborate product identification, the product mixture was analyzed on a Hewlett Packard GC–MS instrument.

3. Results and discussion

3.1. Supports

A zirconia-containing SBA-15 support was prepared from purely siliceous SBA-15 by chemical grafting technique using a previously described procedure [16]. Zirconia loading in the Zr-SBA-15 material was found to be 23 wt.% of ZrO_2 which corresponds well to the SBA-15 support covered with a monolayer of highly dispersed zirconia species. Previously it was reported that the preparation method we used allows one to modify the surface properties of the parent SBA-15 material without significant changes in its typical textural and structural characteristics, such as pore diameter, pore wall thickness, long-range mesopore arrangement (*p6mm* hexagonal symmetry), unit-cell parameter, etc. [16]. In line with this, the characteristic shape of N_2 adsorption–desorption isotherm of SBA-15 and its small-angle XRD pattern are still maintained after ZrO_2 incorporation (Figs. 1 and 2, curves (a)). However, a decrease in some specific (calculated per gram of material) textural characteristics was found after zirconia incorporation into the SBA-15 precursor (Table 1). This decrease in the values of surface area (S_{BET}), micropore area (S_μ), total pore volume (V_P) and micropore volume (V_μ) can be attributed to an increase in the material density after zirconia incorporation into the parent SBA-15.

The changes in the surface characteristics of SBA-15 material after ZrO_2 incorporation can be illustrated by the isoelectric point (IEP) values shown in Table 1. It can be clearly observed that if IEP value of the purely siliceous parent SBA-15 is 2.1, after zirconia incorporation it becomes 3.5, whereas IEP of pure zirconia is equal to 4.1. These results point out that surface of Zr-SBA-15 material should have characteristics intermediate between purely siliceous and purely zirconia counterparts. Above isoelectric point determinations permit estimate average surface coverage of Zr-SBA-15 sample by zirconium oxide. This estimation made according to the

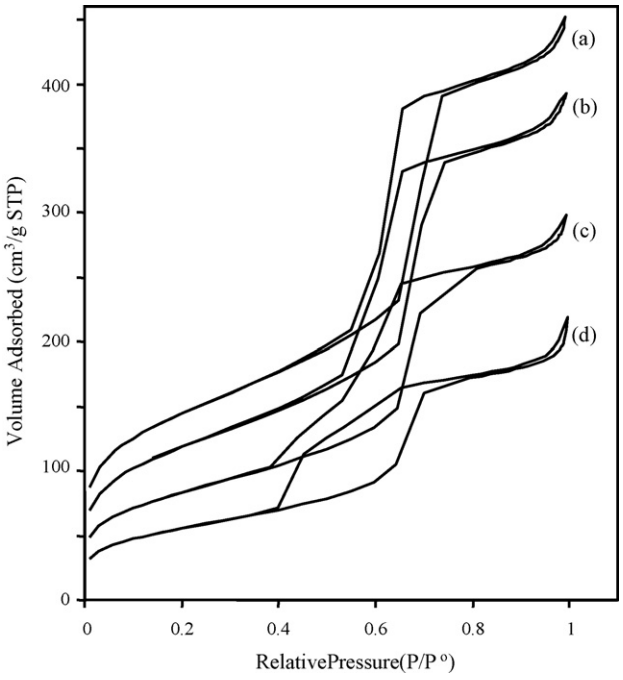

Fig. 1. Nitrogen adsorption–desorption isotherms of Zr-SBA-15 support (a) and corresponding NiMo catalysts with different metal loadings: NiMo(6)/Zr-SBA-15 (b); NiMo(18)/Zr-SBA-15 (c); and NiMo(30)/Zr-SBA-15 (d).

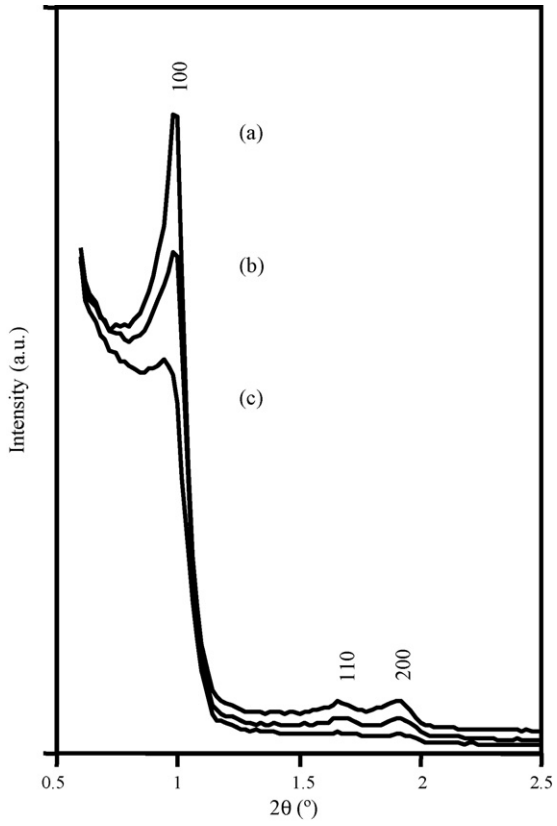

Fig. 2. Small-angle XRD patterns of Zr-SBA-15 support (a), NiMo(12)/Zr-SBA-15 (b) and NiMo(24)/Zr-SBA-15 (c) catalysts.

previously published method [19] indicates that about 84% (~435 m^2/g) of the surface of Zr-SBA-15 is occupied by ZrO_2 species, and the rest of it (16%, ~81 m^2/g) is silica. High surface area of zirconia in the Zr-SBA-15 material prepared in this work, in line with the well-known ability of ZrO_2 to disperse Mo [20,21], allows us to assume that this material should disperse better large amounts of deposited Mo species than its purely siliceous SBA-15 analog, for which the formation of MoO_3 crystalline phase was detected at 12 wt.% of MoO_3 charge (see for example Fig. 4).

3.2. Catalysts

Chemical analysis results (Table 2) show that the actual chemical compositions (Ni and Mo loading) of the prepared NiMo catalysts are close to the expected nominal ones, 6, 12, 18, 24 and 30 wt.% MoO_3 and 1.5, 3.0, 4.5, 6.0 and 7.5 wt.% NiO, respectively. The textural characteristics of NiMo(*X*)/Zr-SBA-15 catalysts with different metal loading are shown in Table 2. A significant decrease in BET surface area and total pore volume is observed when Ni and Mo are incorporated to the support. This decrease is more pronounced for the catalysts with high metal content and it cannot be explained taking into account only the weight of deposited Ni and Mo species. For all NiMo catalysts, micropore area decreases much more than the mesopore one. This result indicates that some obstruction of support pores by metal (Ni and Mo) oxidic species can take place. It seems that at low metal loading (below 18 wt.% MoO_3) micropores are obstructed more than larger mesopores. However, at high metal loading both, micro- and mesopores, are significantly blocked.

Fig. 1 shows the N_2 adsorption–desorption isotherms of NiMo/Zr-SBA-15 catalysts with different MoO_3 loading. All isotherms are of type IV according to IUPAC classification. A progressive decrease in the amount of the adsorbed N_2 is observed with an increase in Ni and Mo loading. In addition, a more detailed analysis of the hysteresis loop demonstrates that its shape changes with Ni and Mo loading. Thus, at low MoO_3 loading (6–12 wt.%) the hysteresis loop still maintains its shape characteristic for SBA-15 support (curves (a) and (b), Fig. 1), but as MoO_3 charge is increased, adsorption and desorption branches of the hysteresis loop become less defined and are displaced to lower P/P_0 values. In line with this observation,

Table 1
Textural characteristics and isoelectric points of supports

Sample	S_{BET} (m^2/g)	S_μ (m^2/g)	V_P (cm^3/g)	V_μ (cm^3/g)	D_{ads} (Å)	D_{des} (Å)	IEP[a] (pH)
SBA-15	786	109	1.072	0.042	74	56	2.1
Zr-SBA-15	516	99	0.679	0.040	74	57	3.5
ZrO_2	58	–	0.249	–	144	115	4.1

[a] Isoelectric point.

Table 2
Textural characteristics and chemical compositions of NiMo catalysts

Sample	MoO_3[a] (wt.%)	NiO[a] (wt.%)	S_{BET} (m^2/g)	S_μ (m^2/g)	V_P (cm^3/g)	V_μ (cm^3/g)	D_{ads} (Å)	D_{des} (Å)
NiMo/SBA-15	12.1	3.0	499	67	0.740	0.025	74	55
NiMo(6)/Zr-SBA-15	6.1	1.5	425	57	0.591	0.022	65	57
NiMo(12)/Zr-SBA-15	12.0	2.9	366	46	0.530	0.017	63	54
NiMo(18)/Zr-SBA-15	18.1	4.4	299	34	0.438	0.012	63	54
NiMo(24)/Zr-SBA-15	23.9	6.1	245	27	0.367	0.009	63	49
NiMo(30)/Zr-SBA-15	30.2	7.4	199	22	0.303	0.007	63	45

[a] Determined by SEM-EDX.

mesopore diameters determined from both adsorption and desorption isotherms by BJH method decrease with an increase in Ni and Mo loading (Table 2). However, it seems that adsorption and desorption pore diameters follow different trends with metal charge. Adsorption pore diameter of the initial Zr-SBA-15 support decreases quickly from 74 to 65 and 63 Å in NiMo catalysts with low metal loadings (6 and 12 wt.% MoO_3, respectively). Further increase in Ni and Mo loading (18–30 wt.% MoO_3) does not affect anymore the adsorption pore diameter of the catalysts (D_{ads}), but strongly changes the corresponding value obtained from the desorption isotherm (D_{des}) which decreases to 45 Å at 30 wt.% MoO_3 loading. This behavior of adsorption and desorption pore sizes can be explained considering that at low metal loadings (below 18 wt.% MoO_3) almost all Ni and Mo oxidic species are deposited inside the support mesopores covering pore walls and reducing internal pore diameter. However, when the dispersion capacity of the Zr-SBA-15 support is saturated (at about 18 wt.% MoO_3), metal species in excess start to agglomerate in pore mouths, leading to a quick decrease in their diameter, and on the external surface of the support particles. This result confirms the above supposition about some agglomeration of the deposited metal species which becomes more pronounced with an increase in metal loading.

Small-angle XRD patterns of NiMo catalysts (Fig. 2) are similar to those of support. It can be clearly observed, that the position of the (1 0 0), (1 1 0) and (2 0 0) reflections of *p6mm* hexagonal structure characteristic for SBA-15 did not change after Ni and Mo incorporation indicating that the unit-cell parameter of the support was preserved in NiMo catalysts with different metal loading. However, the intensities of the three reflections of Zr-SBA-15 support decrease notably when metal loading is increased. Therefore, a slight decrease in long-range periodicity order of the support pores can be expected after Ni and Mo incorporation, especially in the samples with high metal content.

Additional information about the coordination and aggregation state of Ni and Mo oxidic species in catalysts with different metal loading was obtained by UV–vis diffuse reflectance spectroscopy and wide-angle XRD. Fig. 3 shows DRS spectra of five NiMo catalysts supported on Zr-SBA-15. As it was reported previously, Zr-SBA-15 support shows one absorption band with a maximum at 200 nm [16]. Since the spectrum of the Zr-SBA-15 support was subtracted from the spectrum of each examined NiMo catalyst, absorption in the 200–350 nm region observed in Fig. 3 should be assigned only to ligand-to-metal charge transfer (LMCT) $O^{2-} \rightarrow Mo^{6+}$. It is well-known that the position of this LMCT band depends strongly on the local symmetry around the Mo^{6+} species and their aggregation state. The isolated molybdate species in tetrahedral coordination (Mo(Td)) show a characteristic absorption band at ~250 nm, whereas the signal of polymolybdate species in octahedral coordination (Mo(Oh)) is observed at the 280–330 nm region and its position is affected by the aggregate size (the larger aggregates have the smaller energies) [22]. In addition, both types of Mo^{6+} species show the second strong absorption band at about 220 nm. The DRS spectra of our NiMo(*X*)/Zr-SBA-15

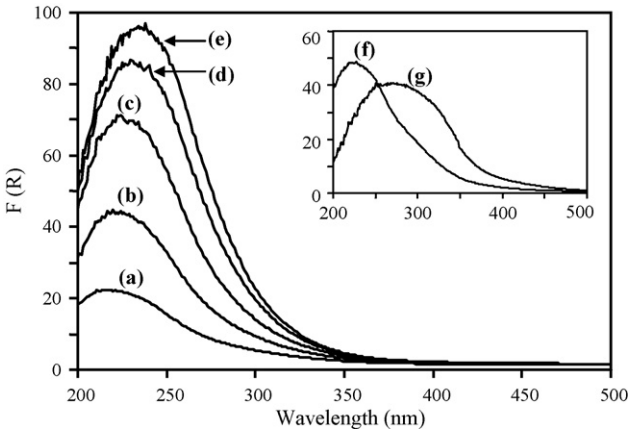

Fig. 3. UV–vis diffuse reflectance spectra of NiMo/Zr-SBA-15 catalysts with different metal loadings: 6 wt.% MoO_3 (a); 12 wt.% MoO_3 (b); 18 wt.% MoO_3 (c); 24 wt.% MoO_3 (d); and 30 wt.% MoO_3 (e). For comparison the spectra of NiMo/SBA-15 (f) and NiMo/γ-Al_2O_3 (g) samples are shown inset.

catalysts (curves (a)–(e), Fig. 3) reveal the presence of a mixture of Mo^{6+} oxidic species in tetrahedral and octahedral coordinations. As metal loading in the catalyst is increased, a red shift of the Mo absorption edge is observed reflecting an increase in the agglomeration of Mo(Oh) species. However, it should be mentioned that the polymolybdate species are much better dispersed on the surface of ZrO_2-modified SBA-15 material than on purely siliceous SBA-15 or conventional γ-Al_2O_3 support (spectra (f) and (g) shown inset in Fig. 3).

Powder XRD patterns for Mo and NiMo/Zr-SBA-15 catalysts with different metal loading are shown in Fig. 4. Zr-SBA-15 support prepared in this work does not show the presence of any crystalline phase. Therefore, all sharp signals observed in Fig. 4 should correspond only to deposited Mo and Ni oxidic species. Indeed, all of them can be assigned to orthorhombic MoO_3 crystalline phase (JCPDS card 35–609). In the diffractograms of unpromoted Mo catalysts, the signals of this crystalline phase can be detected for MoO_3 loadings larger than 12 wt.%. Addition of Ni to Mo(*X*)/Zr-SBA-15 catalysts significantly improves the dispersion of oxidic Mo species. However, small reflections of the crystalline MoO_3 phase can still be detected in Fig. 4 in the XRD patterns of high loading NiMo catalysts (24 and 30 wt.% MoO_3). XRD results, in line with DRS observations, point out the progressive increase in the agglomeration of the oxidic Mo species with metal loading even in the case of Ni-promoted samples. This conclusion was also confirmed by the results from TPR characterization of the catalysts.

The TPR results for Mo and NiMo catalysts with different metal loading are shown in Fig. 5. The TPR profiles of the Mo(*X*)/Zr-SBA-15 exhibit a main reduction peak at the 520–560 °C region that can be ascribed to the first step of reduction (from Mo^{6+} to Mo^{4+}) of polymeric octahedral Mo species [23]. Slight increase in the temperature of the maximum of this peak with Mo loading can be associated with an increase in the agglomeration of octahedral Mo species with metal charge. In addition, as Mo loading is increased, the hydrogen consumption at high-temperature region (650–800 °C) increases. Two

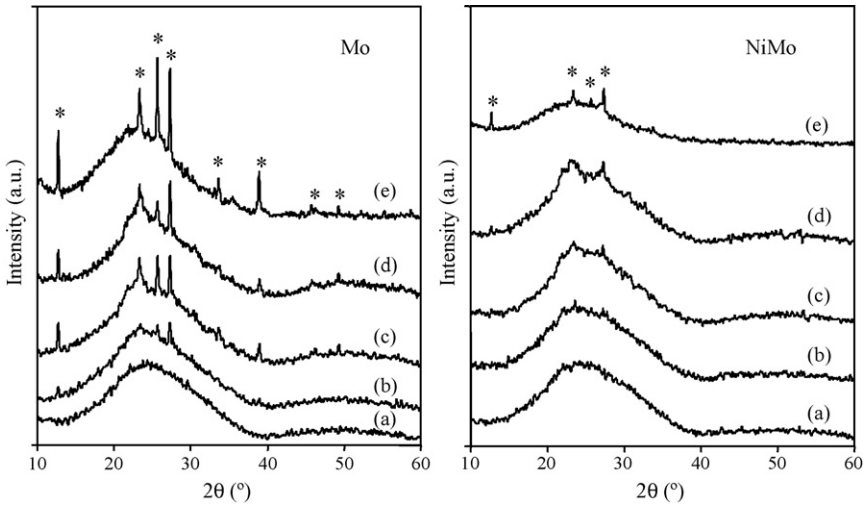

Fig. 4. Powder X-ray diffraction patterns of Mo and NiMo catalysts with different metal loadings supported on Zr-SBA-15: 12 wt.% MoO_3 (a); 18 wt.% MoO_3 (b); 24 wt.% MoO_3 (c); and 30 wt.% MoO_3 (d). For comparison XRD patterns of Mo and NiMo/SBA-15 catalysts (e) are present (*) MoO_3, JCPDS card 35-609.

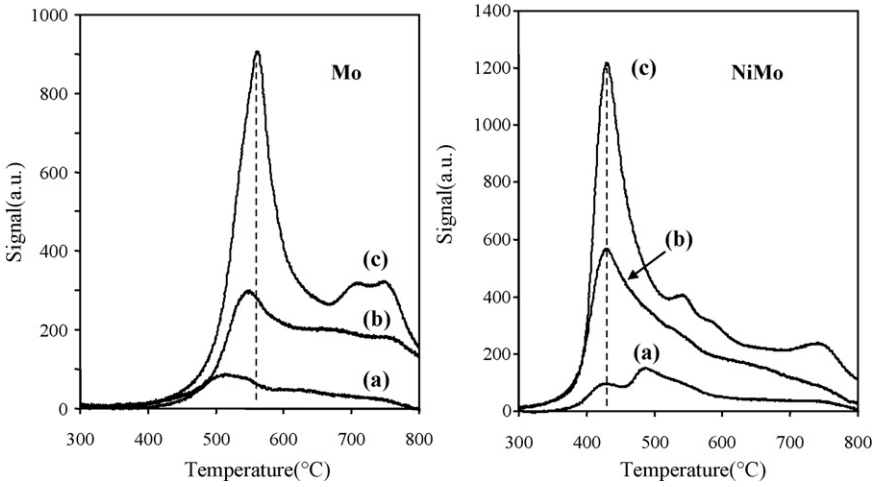

Fig. 5. TPR profiles for Mo(X)/Zr-SBA-15 and NiMo(X)/Zr-SBA-15 catalysts with different metal loadings: 6 wt.% MoO_3 (a); 12 wt.% MoO_3 (b); and 24 wt.% MoO_3 (c).

defined peaks (at 713 and 751 °C) can be observed in the TPR profile of Mo(24)/Zr-SBA-15 catalyst (Fig. 5). One of them can be ascribed to the second step of reduction of the polymeric octahedral Mo species (from Mo^{4+} to Mo^0) and the other, to the first step of reduction of tetrahedral Mo^{6+} species in strong interaction with ZrO_2-containing support. The presence of such tetrahedral Mo species is in line with our DRS results described above, as well as, with previously published reports [20,24] in which the presence of isolated tetrahedral MoO_x species was detected in Mo catalysts supported on pure zirconia by Raman spectroscopy. In the TPR profiles of NiMo(*X*)/Zr-SBA-15 catalysts the reduction of Mo species occurs at lower temperatures than in unpromoted Mo catalysts indicating, in accordance with the powder XRD results, better dispersion of Mo species in the presence of Ni. It was also observed that the proportion of dispersed octahedral Mo species, which reduce at low temperatures (350–500 °C) is higher in NiMo catalysts in comparison with the respective Mo catalysts. Therefore, Ni addition promotes the dispersion of oxidic Mo species and makes easier their reduction. In addition, in the TPR profile of the NiMo(6)/Zr-SBA-15 catalyst a reduction peak at 480 °C can be clearly observed which is attributable to the reduction of $NiMoO_4$ (main reduction peak at 475 °C) [25].

HRTEM observations of the sulfided catalysts reflect the changes in the morphology of MoS_2 with increasing MoO_3 loading. The typical fringes due to MoS_2 crystallites with 6.1 Å interplanar distances were observed on micrographs of all sulfided catalysts (Fig. 6). It can be seen that in the catalyst with low metal loading (6 wt.% MoO_3) supported on Zr-SBA-15, small MoS_2 crystallites with length between 20 and 30 Å and stacking from one to three layers are formed (Fig. 6(a)). An increase in MoO_3 loading leads, as expected, to a worse dispersion of the active phase which is reflected in an increase in length and stacking of MoS_2 particles. Thus, in the micrograph of NiMo(18)/Zr-SBA-15 catalyst (Fig. 6(b)), MoS_2 crystallites with length between 25 and 40 Å and

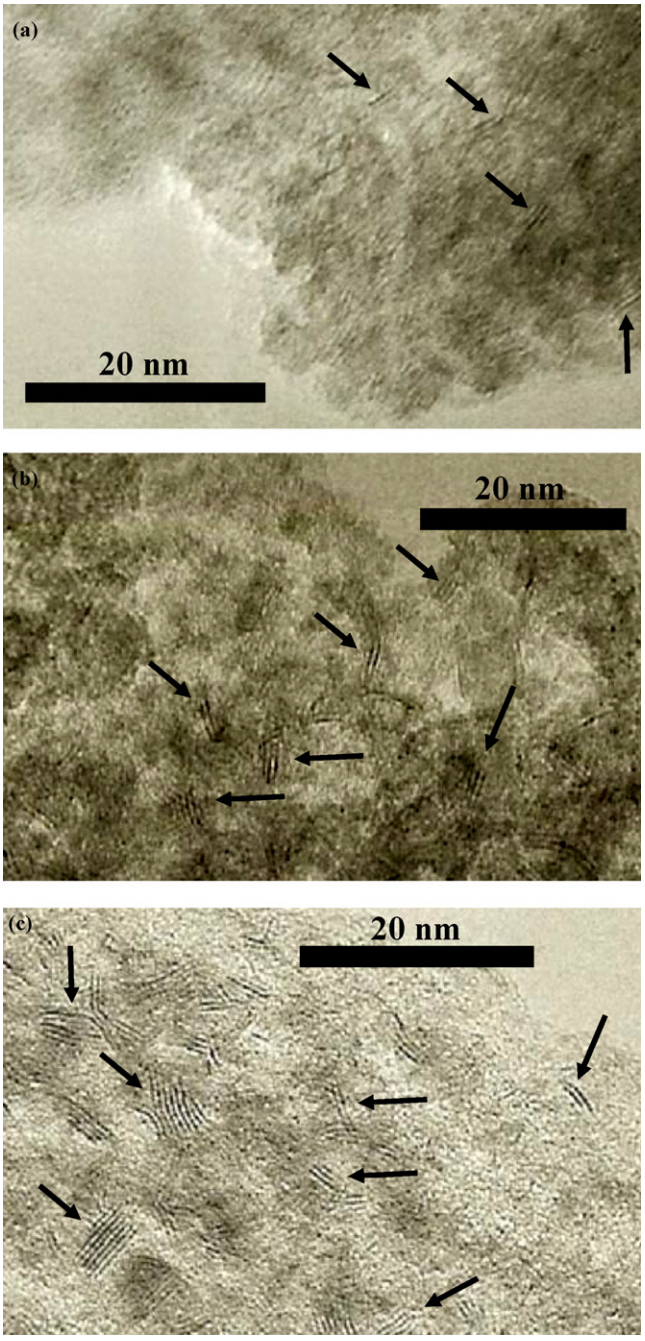

Fig. 6. HRTEM micrographs of sulfided catalysts: NiMo(6)/Zr-SBA-15 (a); NiMo(18)/Zr-SBA-15 (b); and NiMo(30)/Zr-SBA-15 (c).

stacking of 2–4 layers are observed. Further increase in MoO_3 loading to 30 wt.% (Fig. 6(c)) results in a further increase in the size of MoS_2 particles to 25–50 Å length and 2–8 layers. Therefore, HRTEM characterization of the sulfided NiMo(*X*)/Zr-SBA-15 catalysts shows a progressive increase in the size of Mo species with metal loading, similar as it was detected for the oxidic precursors of these catalysts by other characterization methods. However, it should be mentioned that in general in Zr-SBA-15-supported catalysts the dispersion of the MoS_2 active phase is much better and more homogeneous than in the catalysts with similar metal loading supported on purely siliceous SBA-15. For example, as it was reported previously [16], the inhomogeneous distribution of MoS_2 particles was observed for NiMo/SBA-15 catalyst with 12 wt.% MoO_3 and 3 wt.% NiO. Particles with length between 20 and 60 Å and stacking from two to six layers were coexisting with larger MoS_2 crystals located on the external surface of the purely siliceous support. In addition, the comparison of the morphology of MoS_2 active phase on Zr-containing SBA-15 supports and on the conventional γ-alumina [26,27] shows that MoS_2 crystallites in our catalysts are shorter and with larger stacking degree than γ-Al_2O_3-supported analogs.

3.3. Catalytic activity

The catalytic activity of sulfided NiMo(*X*)/Zr-SBA-15 catalysts was examined in the hydrodesulfurization of 4,6-dimethyldibenzothiophene. The conversions of 4,6-DMDBT obtained over different catalysts at various reaction times, as well as corresponding pseudo-first-order rate constants are shown in Table 3. Results obtained with NiMo catalysts (12 wt.% MoO_3, 3 wt.% NiO) supported on purely siliceous SBA-15 and conventional γ-alumina are also shown for comparison purposes. Catalytic activities of all NiMo(*X*) catalysts supported on Zr-modified SBA-15 resulted to be higher than those of the reference NiMo/γ-Al_2O_3 catalyst (prepared in this work) and the commercial CoMo/γ-Al_2O_3 catalyst for which the rate constant value of 4.9×10^{-6} L/(s × g of catalyst) was reported previously [28]. Moreover, catalytic activity of NiMo(*X*)/Zr-SBA-15 catalysts increases with Mo loading reaching a maximum with the catalyst containing 18 wt.% MoO_3 and 4.5 wt.% NiO. This catalyst was almost twice more active than the alumina supported counterparts. However, further increase in MoO_3 loading results in a

Table 3
4,6-DMDBT conversions obtained over different NiMo catalysts and pseudo-first-order rate constants obtained for 4,6-DMDBT HDS over NiMo catalysts

Catalyst	4,6-DMDBT conversion (%)[a]				Pseudo-first-order rate constant, L/(s × g of catalyst)
	2	4	6	8	
NiMo/SBA-15	12	27	43	56	5.01×10^{-6}
NiMo(6)/Zr-SBA-15	18	42	64	79	8.71×10^{-6}
NiMo(12)/Zr-SBA-15	30	58	81	92	1.48×10^{-5}
NiMo(18)/Zr-SBA-15	37	65	84	95	1.88×10^{-5}
NiMo(24)/Zr-SBA-15	29	52	72	90	1.19×10^{-5}
NiMo(30)/Zr-SBA-15	25	48	70	85	1.11×10^{-5}
Reference NiMo/γ-Al_2O_3	11	28	48	61	5.19×10^{-6}

[a] At different reaction time (h).

slight decrease of 4,6-DMDBT conversion and a value of the corresponding rate constant. This trend in the activity of the NiMo catalysts with metal (Mo, Ni) loading should be related to the dispersion of oxidic and sulfided Mo active species. As it was shown above, the oxidic Mo species are still well-dispersed up to 18 wt.% MoO_3 charge. Further increase in Mo loading (24 and 30 wt.% MoO_3) leads to a notable agglomeration of Mo phase with the formation of crystalline MoO_3 (XRD), as well as to an increase in the size of the sulfided Mo particles (HRTEM). It seems that the capacity of the Zr-SBA-15 support used in this work to disperse well Ni-promoted Mo species is reached at MoO_3 loadings between 18 and 24 wt.%. The molar ratio MoO_3:ZrO_2 is equal to 0.86 and 1.27 for NiMo(18) and NiMo(24)/Zr-SBA-15 catalysts, respectively. Therefore, it can be supposed that the dispersion capacity of the Zr-SBA-15 support is reached when the amount of the deposited Mo species is near to 1 Mo atom per 1 atom of Zr on the support surface. This result seems to be reasonable from the point of view of the below considerations. It is well-known that molybdenum interacts with surface hydroxyl groups of supports like alumina, silica, titania, zirconia, etc. [29]. Taking into account that the Zr-SBA-15 support was prepared by chemical grafting method and the ZrO_2 content corresponds well with SBA-15 support covered with a monolayer of dispersed ZrO_2 species, almost all hydroxyl groups of the parent purely siliceous SBA-15 material available for the interaction with Zr (IV) propoxide reacted with it and disappeared. New hydroxyl groups related to the grafted Zr(IV) species should be the principal sites for molybdenum anchoring. These Zr(IV)-related hydroxyl groups are more basic than those of the parent silica that should provide a stronger Mo-support interaction. Therefore, it seems that the amount of grafted zirconium species and corresponding Zr-OH groups will determine the amount of Mo species which can be dispersed on the support like ZrO_2-grafted SBA-15. However, this supposition needs a further experimental confirmation.

It is known that the HDS of 4,6-dimethyldibenzothiophene occurs through two parallel reaction routes as shown in Fig. 7. The first one is called the direct desulfurization (DDS) pathway and comprises direct elimination of S atom via C–S bond cleavage yielding the corresponding dimethylbiphenyl (DMBP) product. The second, usually called the hydrogenation (HYD) pathway, consists in the hydrogenation of one of the benzene rings of 4,6-DMDBT followed by hydrogenolysis. This pathway yields first tetrahydrodimethyldibenzothiophene (THDBT), then the corresponding hexahydro-derivative (HHDBT) and, finally, methylcyclohexyltoluene (MCHT). The ratio between the two reaction pathways depends on both the nature of the S-containing molecule and the catalyst. In the case of 4,6-dimethyldibenzothiophene, desulfurization mainly occurs via the HYD route [30,31]. Previously, it was concluded from a study of different unsupported MoS_2 catalysts that there are two different active sites involved in the HDS activity [32]. One is active in the hydrogenation reactions and the other one in hydrogenolysis. Computer modeling and simulation of 4,6-DMDBT adsorption and its interaction with the active sites of the catalyst surface have been applied to understand the reaction pathways and mechanism. It was demonstrated that there are two possible configurations for 4,6-DMDBT chemisorption on MoS_2 surface, the flat adsorption (π-adsorption of benzenic rings) and plug-in adsorption by the sulfur atom (S-μ_3) [31]. Recently, it was shown by density-functional calculations that the hydrogenation pathway should start from the flat adsorption of 4,6-DMDBT on the molybdenum edge of the active phase whereas the direct desulfurization of the DBT molecules should involve the plug-in adsorption on the sulfur edge [33]. The last type of adsorption is inhibited for 4,6-DMDBT due to steric hindrance generated by the methyl groups at the positions 4 and 6, therefore, the DDS pathway is strongly blocked for this molecule and the HYD pathway becomes preferential. When 4,6-DMDBT has at least one aromatic ring pre-hydrogenated, steric hindrance becomes lower and subsequent desulfurization is enabled. Resuming the above, it can be concluded that in order to desulfurize 4,6-DMDBT via the HYD pathway, the catalyst needs to have both types of active sites, namely, the sites for hydrogenation of the initial 4,6-DMDBT molecule and the sites for the desulfurization of the pre-hydrogenated 4,6-DMDBT intermediates (Fig. 7). The over-all efficiency of the HYD route should also depend on the balance between the hydrogenation sites on the molybdenum edges and the hydrogenolysis sites on the sulfur edges of the MoS_2 particles. HRTEM results described above show that the morphology of the MoS_2 active phase changes with metal loading in the catalysts. In line with this, the total amount of the catalyst active sites, as well as the ratio between different types of adsorption sites should also depend on the metal loading.

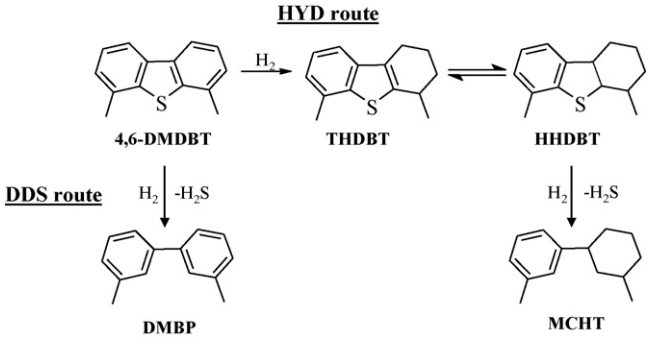

Fig. 7. Reaction network for 4,6-dimetyldibenzothiophene hydrodesulfurization. THDBT, tetrahydrodimethyldibenzothiophene; HHDBT, hexahydrodimethyldibenzothiophene; MCHT, methylcyclohexyltoluene; DMBP, dimethylbiphenyl.

The reaction product distributions at the same total 4,6-DMDBT conversion (50%) were compared for all catalysts. The ratios between different products involved in the reaction network of 4,6-DMDBT hydrodesulfurization are present in Table 4. The ratio of the pre-hydrogenated derivatives of 4,6-DMDBT to dimethylbiphenyl product reflects the ratio of the sites able to adsorb the reactant molecule in a flat form to those suitable for its plug-in adsorption. It can be seen that for all evaluated catalysts (with the exception of NiMo(6)/Zr-SBA-15) the proportion of the hydrogenated intermediates is higher than that of the biphenyl-type product. Moreover, for a series of

Table 4
Reaction product ratios obtained over NiMo catalysts at 50% of total 4,6-DMDBT conversion

Catalyst	(THDBT + HHDBT)/DMBP	(THDBT + HHDBT)/MCHT	MCHT/DMBP[a]
NiMo/SBA-15	1.90	0.34	6.6
NiMo(6)/Zr-SBA-15	0.94	0.17	6.6
NiMo(12)/Zr-SBA-15	1.34	0.17	7.6
NiMo(18)/Zr-SBA-15	1.54	0.27	8.0
NiMo(24)/Zr-SBA-15	1.62	0.29	5.8
NiMo(30)/Zr-SBA-15	1.73	0.27	6.4
Reference NiMo/γ-Al_2O_3	1.34	0.16	9.6

[a] THDBT, tetrahydrodimethyldibenzothiophene; HHDBT, hexahydrodimethyldibenzothiophene; MCHT, methylcyclohexyltoluene; DMBP, dimethylbiphenyl.

NiMo/Zr-SBA-15 catalysts this proportion progressively increases with the MoO_3 loading. This behavior seems to be in line with the increase in stacking degree of MoS_2 active phase with metal loading detected by HRTEM. This result is in accordance with previous reports [14,34], in which an increase in HYD rate was observed with an increasing MoS_2 stacking, and it was attributed to a less hampered planar adsorption geometry of reactants on multilayered MoS_2 particles. The highest value of the ratio of the hydrogenated intermediates of 4,6-DMDBT to DMBP has been obtained for the NiMo/SBA-15 catalyst. The same catalyst also shows the highest ratio of (THDBT + HHDBT) to the corresponding desulfurized product (MCHT). It seems that this catalyst has many hydrogenation sites but only a small amount of the hydrogenolysis ones. On the contrary, reference NiMo catalyst supported on γ-alumina shows relatively high proportion of desulfurized products (DMBP and MCHT) in comparison with hydrogenated derivatives of 4,6-DMDBT. This catalyst has very good hydrogenolysis ability, but the amount of HYD active sites seems to be small. In the case of NiMo(*X*)/Zr-SBA-15 samples, the proportion of hydrogenation/hydrogenolysis sites progressively changes when metal loading is increased. Product ratios from Table 4 show that the amount of HYD sites increases with Mo charge, whereas the amount of hydrogenolysis sites decreases at the same time. The most active catalyst, NiMo(18)/Zr-SBA-15, shows intermediate values of both ratios (THDBT + HHDBT)/DMBP and (THDBT + HHDBT)/MCHT. Probably, the high activity of this catalytic formulation is due to the best balance between two types of HDS active sites involved in the HYD pathway of hydrodesulfurization.

Finally, it can be mentioned that for all catalysts (THDBT + HHDBT)/MCHT ratio is much smaller than (THDBT + HHDBT)/DMBP, that is in line with the above-mentioned supposition that the elimination of the sulfur atom through C–S bond cleavage should be easier from partially hydrogenated intermediates than from the initial 4,6-DMDBT molecule.

4. Conclusions

According to the above results, the following conclusions can be stated:

Zirconia incorporation on the SBA-15 surface improves the dispersion of the Ni-promoted oxidic and sulfided Mo species, which were found to be highly dispersed, up to 18 wt.% of MoO_3 loading (XRD, DRS, TPR, HRTEM). Further increase in metal charge resulted in the formation of MoO_3 crystalline phase (XRD) and a decrease in the dispersion of the MoS_2 particles (HRTEM).

All NiMo catalysts supported on ZrO_2-containing SBA-15 showed high activity in HDS of 4,6-DMDBT, one of the most refractory sulfur compounds. The best catalyst having 18 wt.% of MoO_3 and 4.5 wt.% of NiO was almost twice more active than the commercial CoMo/γ-Al_2O_3 [28] or reference NiMo/γ-Al_2O_3 catalysts. However, further increase in NiO and MoO_3 loading resulted in a slight decrease in 4,6-DMDBT conversions. It seems that the dispersion capacity of the support is reached at about 18–24 wt.% of MoO_3 charge. It was observed that the activity trends of NiMo/Zr-SBA-15 catalysts with different metal loading, as well as their hydrogenation and hydrogenolysis abilities are closely related to the dispersion and morphology (length and stacking degree) of MoS_2 species determined by HRTEM. As metal loading increases, MoS_2 particles become larger and more stacked, consequently, the proportion of hydrogenation/hydrogenolysis active sites changes, the amount of HYD sites increases and the amount of hydrogenolysis sites decreases. It seems that the most active catalyst, NiMo(18)/Zr-SBA-15, has a large amount of HDS active sites and the best balance between two types of active sites involved in the HYD pathway of hydrodesulfurization.

Finally it can be concluded that the activity of NiMo/Zr-SBA-15 catalysts in HDS of refractory sulfur compounds can be improved by increasing the loading level of Mo active phase (up to 18 wt.% MoO_3).

Acknowledgements

Financial support by CONACYT-Mexico (grant 46354-Y) is gratefully acknowledged. The authors thank M. Aguilar Franco, C. Salcedo Luna and I. Puente Lee for technical assistance with XRD and HRTEM characterizations.

References

[1] C. Song, Catal. Today 86 (2003) 211.
[2] L. Vradman, M.V. Landau, M. Herskowitz, Catal. Today 48 (1999) 41.
[3] K.G. Knudsen, B.H. Cooper, H. Topsøe, Appl. Catal. A: Gen. 189 (1999) 205.
[4] A. Ishihara, F. Dumeignil, J. Lee, K. Mitsuhashi, E.W. Qian, T. Kabe, Appl. Catal. A: Gen. 289 (2005) 163.

[5] F. Dumeignil, K. Sato, M. Imamura, N. Matsubayashi, E. Payen, H. Shimada, Appl. Catal. A: Gen. 315 (2006) 18.
[6] M. Nagai, T. Fukiage, S. Kurata, Catal. Today 106 (2005) 201.
[7] E. Kraleva, A. Spojakina, K. Jiratova, L. Petrov, Catal. Lett. 112 (2006) 203.
[8] Y. Okamoto, M. Breysse, G.M. Dhar, C. Song, Catal. Today 86 (2003) 1.
[9] D. Zhao, J. Feng, Q. Huo, N. Melosh, G.H. Fredrickson, B.F. Chmelka, G.D. Stucky, Science 279 (1998) 548.
[10] D. Zhao, Q. Huo, J. Feng, B.F. Chmelka, G.D. Stucky, J. Am. Chem. Soc. 120 (1998) 6024.
[11] A. Sampieri, S. Pronier, J. Blanchard, M. Breysse, S. Brunet, K. Fajerwerg, C. Louis, G. Pérot, Catal. Today 107/108 (2005) 537.
[12] G. Murali Dhar, G. Muthu Kumaran, M. Kumar, K.S. Rawat, L.D. Sharma, B. David Raju, K.S. Rama Rao, Catal. Today 99 (2005) 309.
[13] L. Vradman, M.V. Landau, M. Herskowitz, V. Ezersky, M. Talianker, S. Nikitenko, Y. Koltypin, A. Gedanken, J. Catal. 213 (2003) 163.
[14] E.J.M. Hensen, P.J. Kooyman, Y. van der Meer, A.M. van der Kraan, V.H.J. de Beer, J.A.R. van Veen, R.A. van Santen, J. Catal. 199 (2001) 224.
[15] G. Muthu Kumaran, S. Garg, K. Soni, M. Kumar, L.D. Sharma, G. Murali Dhar, K.S. Rama Rao, Appl. Catal. A: Gen. 305 (2006) 123.
[16] O.Y. Gutiérrez, G.A. Fuentes, C. Salcedo, T. Klimova, Catal. Today 116 (2006) 485.
[17] O.Y. Gutiérrez, K.A. Romero, G.A. Fuentes, T. Klimova, Stud. Surf. Sci. Catal. 162 (2006) 355.
[18] G. Murali Dhar, S. Garg, G.M. Kumaran, K. Soni, V.V.D.N. Prasad, J.K. Gupta, Prep. Pap. Am. Chem. Soc., Div. Petrol. Chem. 51 (1/2) (2006).
[19] F.J. Gil Lliambas, L. Bouyssieres, A. López Agudo, Appl. Catal. 65 (1990) 45.
[20] S. Xie, K. Chen, A.T. Bell, E. Iglesia, J. Phys. Chem. B 104 (2000) 10059.
[21] E. Payen, L. Gengembre, F. Mauge, J.C. Duchet, J.C. Lavalley, Catal. Today 10 (1991) 521.
[22] R.S. Weber, J. Catal. 151 (1995) 470.
[23] R. López Cordero, F.J. Gil Llambias, A. López Agudo, Appl. Catal. 74 (1991) 125.
[24] M. Jia, P. Afanasiev, M. Vrinat, Appl. Catal. A: Gen. 278 (2005) 213.
[25] J.L. Brito, J. Laine, J. Catal. 139 (1993) 540.
[26] T. Klimova, D. Solís Casados, J. Ramírez, Catal. Today 43 (1998) 135.
[27] E. Payen, R. Hubaut, S. Kasztelan, O. Poulet, J. Grimblot, J. Catal. 147 (1994) 123.
[28] B. Gates, H. Topsøe, Polyhedron 16 (1997) 3213.
[29] H. Topsøe, B.S. Clausen, F.E. Massoth, in: J.R. Anderson, M. Boudart (Eds.), Hydrotreating Catalysis Science and Technology, vol. 11, Springer, New York, 1996, Chap. 3, p. 74.
[30] D.D. Whitehurst, T. Isoda, I. Mochida, Adv. Catal. 42 (1998) 345.
[31] C. Song, X. Ma, Appl. Catal. B: Env. 41 (2003) 207.
[32] H. Farag, K. Sakanishi, M. Kouzu, A. Matsumura, Y. Sugimoto, I. Saito, J. Mol. Catal. A: Chem. 206 (2003) 399.
[33] S. Cristol, J.-F. Paul, E. Payen, D. Bougeard, F. Hutschka, S. Clémendot, J. Catal. 224 (2004) 138.
[34] P. Da Silva, N. Marchal, S. Kasztelan, Stud. Surf. Sci. Catal. 106 (1997) 353.